# Synthesis and study of the crystallographic and magnetic structure of $SeCoO_3$

A. Muñoz*
*Departamento de Física Aplicada, EPS, Universidad Carlos III, Avda. Universidad 30, E-28911, Leganés-Madrid, Spain*

J. A. Alonso and M. J. Martínez-Lope
*Instituto de Ciencia de los Materiales de Madrid, CSIC, E-28049, Cantoblanco-Madrid, Spain*

E. Morán
*Departamento de Química Inorgánica, Facultad de C.C. Químicas, Universidad Complutense de Madrid, Ciudad Universitaria, E-28040 Madrid, Spain*

R. Escamilla
*Instituto de Investigaciones en Materiales, Universidad Autónoma de México, 04510 México DF, México*
(Received 27 October 2005; revised manuscript received 15 February 2006; published 27 March 2006)

We describe the preparation of $SeCoO_3$ under moderate pressure conditions (3.5 GPa), starting from reactive $SeO_3H_2$ and MO mixtures, contained in sealed gold capsules under the reaction conditions (850 °C for 1 h). The sample has been studied by neutron powder diffraction (NPD) data, specific heat, and magnetization measurements. $SeCoO_3$ is an orthorhombically distorted perovskite (space group *Pnma*), with unit cell parameters $a=5.9300(2)$, $b=7.5961(2)$, $c=5.0287(2)$ Å. Below $T_N \approx 54$ K it experiences an antiferromagnetic ordering, as demonstrated by susceptibility and NPD measurements. Above the Néel temperature, a paramagnetic moment of 5.3 $\mu_B$/f.u. (expected is 5.2 for $Co^{2+}$ in $^4T_{1g}$) and $\theta_{Weiss}=-86.7$ K are obtained from the reciprocal susceptibility. Below $T_N$, the magnetic reflections observed in the neutron patterns can be indexed with a propagation vector $\mathbf{k}=0$, thus the magnetic unit cell coincides with the chemical one. The magnetic structure is given by the basis vectors $(\mathbf{A_x}, \mathbf{G_y}, \mathbf{0})$ and it remains stable down to 2.2 K. The $Co^{2+}$ moments are lying on the $(a,b)$ plane of the perovskite; the structure is noncollinear but noncanted. There exists perfect AFM interactions (180°) between moments within the $(c,a)$ plane (via O2 oxygens), whereas the magnetic moments exhibit angles of about 90° along the **b** axis (via O1 oxygens). At low temperatures (2 K) the $Co^{2+}$ ordered saturation moment is of 3.4 $\mu_B$, which is consistent with high spin $Co^{2+}$ $(3t_{2g}^5 e_g^2)$.

DOI: 10.1103/PhysRevB.73.104442 PACS number(s): 75.25.+z

## I. INTRODUCTION

The compounds of the family of $(Se,Te)MO_3$ ($M$ =divalent transition metal) perovskites have the particularity of containing Se(IV) or Te(IV), with a lone electron pair, at the A positions of the $ABO_3$ perovskite structure, usually occupied by voluminous cations. This gives rise to strongly tilted $MO_6$ octahedra with rather bent $M$-O-$M$ superexchange $\phi$ angles, which account for the surprising magnetic properties described for these materials.[1] For instance, in the $Se_{1-x}Te_xCuO_3$ series[2] the magnetic interactions can be tuned between ferromagnetic, for $SeCuO_3$, exhibiting $\phi$ angles of 121°, and antiferromagnetic for $TeCuO_3$, with $\phi=131°$, as demonstrated by magnetic susceptibility measurements.[3] The effect of cationic substitutions in the B sublattice of the perovskite has also been studied, as in the $Se(Cu_{1-x}Mn_x)O_3$ series,[4] where a sharp drop in the magnetization and a change from positive to negative Weiss constant is observed upon Mn doping.

However, the microscopic origin of this behavior has not been investigated much so far.[5] In fact, the magnetic structures of the compounds of the $SeMO_3$ ($M$=Mn, Co, Ni, Cu) series have not been described. The lack of accurate neutron diffraction measurements probably arises from the fact that all the samples of the $(Se,Te)MO_3$ family require high pressure preparation conditions (6–8 GPa), necessary to stabilize the strongly distorted perovskite structures, providing insufficient amounts of sample.

In this work, we describe the preparation of the $M$=Co member of the series, $SeCoO_3$ obtained under moderate pressure conditions (3.5 GPa), starting from reactive $H_2SeO_3$ and MO mixtures, and the results of a neutron powder diffraction (NPD) study complemented with magnetization and specific heat measurements. $SeCoO_3$ had been previously described as an antiferromagnet with $T_N=49(1)$ K.[1] It was reported as an orthorhombically distorted perovskite (space group *Pnma*) with unit cell parameters $a=5.9297(4)$, $b=7.5954(4)$, and $c=5.0293(2)$ Å, from x-ray diffraction data.

## II. EXPERIMENT

About 1 g of a stoichiometric mixture of $H_2SeO_3$ and CoO was thoroughly ground and put into a platinum capsule (6 mm diam), sealed and placed in a cylindrical graphite heater. The reaction was carried out in a piston-cylinder press (Rockland Research Co.), at a pressure of 3.5 GPa at 850 °C for 1 h. Then the material was quenched to room temperature and the pressure was subsequently released.

The product was initially characterized by laboratory XRD (Cu $K\alpha$, $\lambda=1.5406$ Å) for phase identification and to assess phase purity. For the structural refinements, NPD pat-

 

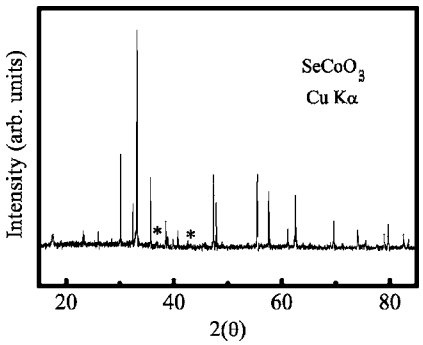


FIG. 1. XRD pattern of $SeCoO_3$; the star indicates the most intense reflections of the CoO impurity.

terns were collected at room temperature (295 K) and 5 K at the high resolution D2B neutron diffractometer of ILL-Grenoble. In spite of the relatively small amount of sample available (about 0.6 g), a good quality pattern could be collected with the high-flux mode and a counting time of 4 h for each pattern. A wavelength of 1.594 Å was selected from a Ge monochromator. Low temperature medium-resolution NPD patterns were collected at the D20 diffractometer with $\lambda=2.40$ Å, in order to follow the thermal evolution of the magnetic structure. The sample was placed in a standard orange cryostat and cooled down to 2.2 K; then sequential NPD diagrams were collected during the heating run, at 0.4 K $min^{-1}$, in the 2.2–72.7 K temperature range, with a counting time of 15 min per diagram. All the patterns were refined by the Rietveld method,[6] using the FULLPROF refinement program.[7] A pseudo-Voigt function was chosen to generate the line shape of the diffraction peaks. No regions were excluded in the refinement. In the final run the following parameters were refined from the high-resolution D2B data: scale factor, background coefficients, zero-point error, unit-cell parameters, pseudo-Voigt corrected for asymmetry parameters, positional coordinates, isotropic thermal factors, and magnitude of the Co magnetic moments. The coherent scattering lengths for Se, Co, and O were 7.97, 2.49, and 5.803 fm, respectively. The magnetic form factors considered for $Co^{2+}$ cations were determined with the coefficients taken from the International Tables of Crystallography.

The magnetic measurements were performed in a commercial superconducting quantum interference device magnetometer (SQUID). The dc magnetic susceptibility curve was obtained in the temperature range $1.8<T<300$ K under a 1 kOe magnetic field. Magnetization isotherms were measured at $T=1.8$, 21, 42, and 80 K, for magnetic fields ranging from −50 kOe to 50 kOe. For the measurements of the specific heat, a semiadiabatic He calorimeter based in the heat-pulsed method was used; different specific heat curves were obtained under a 0, 40, and 90 kOe and in the temperature intervals 1.9–202 K, 1.9–89.8 K, and 1.9–104.0 K, respectively.

## III. RESULTS

The $SeCoO_3$ sample was obtained as a violet polycrystalline powder. The XRD pattern (Fig. 1) is characteristic of a well crystallized perovskite, which can be indexed in an orthorhombic unit cell with $a=5.9300(2)$, $b=7.5961(2)$, $c=5.0287(2)$ Å, space group *Pnma*. These parameters are comparable with those given in Ref. 1. An impurity phase of CoO was detected, as indicated in Fig. 1 with a star.

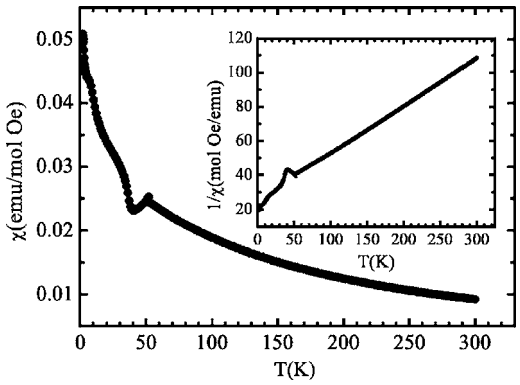


FIG. 2. Thermal evolution of the dc susceptibility measured under a 1 kOe magnetic field. Inset: thermal evolution of the inverse of the susceptibility.

### A. Magnetic measurements

The thermal variation of the dc susceptibility measured under a 1 kOe magnetic field is displayed in Fig. 2. On decreasing the temperature a first anomaly appears in the curve at around 54 K, which could be ascribed to the onset of an antiferromagnetic order with $T_N \approx 54$ K. On cooling below $T_N$ the susceptibility decreases, as it would correspond to the onset of an antiferromagnetic order, but around 35 K, the susceptibility undergoes an abrupt increase. As it will be shown in the analysis of the neutron diffraction measurements, no changes are observed in the magnetic structure of $SeCoO_3$ that can explain this increase. Therefore, this behavior could be attributed to the presence of traces of $Co_3O_4$, that orders just below $T_N=35$ K,[8] in very small amounts that have not been detected in the NPD patterns. The inverse of the dc susceptibility (inset of Fig. 2) presents a linear behavior for temperatures above $T_N$. A fit to the Curie-Weiss Law in the temperature interval $170<T<300$ K yields a paramagnetic temperature $\Theta_P=-84.5(3)$ K and an effective magnetic moment $\mu_{\text{eff}}=5.32(1)\ \mu_B$. $SeCoO_3$ contains $Co^{2+}$ cations ($d^7$), with a ground state $^4T_{1g}$, for which the effective magnetic moment is 5.2 $\mu_B$. In the case that the angular orbital moment is quenched ($J=S$), the effective magnetic moment is only 3.87 $\mu_B$. In the present case, the experimental effective magnetic moment corresponds to a completely unquenched angular orbital moment.

The isothermal magnetization curves are shown in Fig. 3. At $T=2$ K a small hysteresis is observed in the curve, which indicates the presence of a weak ferromagnetic component. In the curves at $T=21$, 42, and 80 K a linear, nonhysteretic $M$ vs $H$ plot is observed, characteristic of an antiferromagnetic or paramagnetic behavior, in agreement with the dc susceptibility and the neutron diffraction data.

### B. Specific heat measurements

The specific heat curves acquired under several magnetic fields are reported in Fig. 4. In the curve under a zero mag-

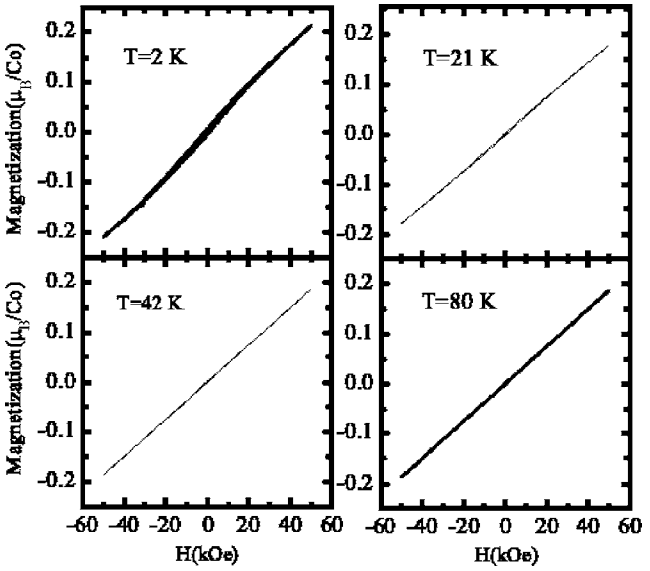


FIG. 3. Isothermal magnetization curves at $T=1.8$, 21, 42, and 80 K.

netic field, a sharp anomaly appears at around $T_N$, corresponding to the onset of long-range magnetic ordering, in good agreement with the magnetic measurements. The specific heat curve is not affected when a 40 kOe magnetic field is applied on the sample. However, under a higher magnetic field, 90 kOe, the peak associated with the magnetic ordering undergoes a small shift to a lower temperature, which is a characteristic feature of an antiferromagnetic long-range ordering.

### C. Neutron diffraction experiments

#### *1. Crystallographic structure*

The crystallographic structure of $SeCoO_3$ has been analyzed from two high resolution NPD patterns collected at room temperature and at $T=5$ K with a $\lambda=1.594$ Å wavelength. The structure was defined in the orthorhombic space group *Pnma* (No. 62), $Z=4$, with unit-cell parameters related to $a_0$ (ideal cubic perovskite, $a_0 \approx 3.8$ Å) as $a \approx c \approx \sqrt{2}a_0$, $b \approx 2a_0$. Se atoms were located at 4*c* positions, Co at 4*b*, and oxygen atoms at 4*c* and 8*d* positions, respectively.

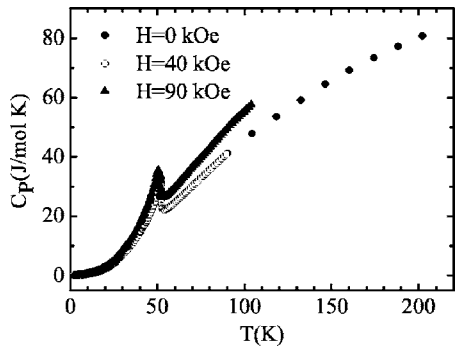


FIG. 4. Thermal variation of the specific heat under a 0, 40, and 90 kOe magnetic field.

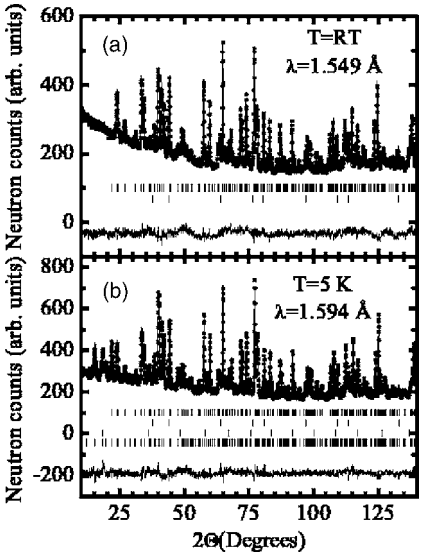


FIG. 5. Experimental (full circles) and calculated (solid line) NPD patterns; the difference is at the bottom. (a) $T=295$ K; the two series of tic marks correspond to the nuclear Bragg reflections of $SeCoO_3$ and CoO, respectively. (b) $T=5$ K; the first and fourth series of marks correspond to the nuclear and magnetic Bragg reflections of $SeCoO_3$, respectively; the second and third ones to the nuclear and magnetic peaks of CoO.

The oxygen stoichiometry at O1 and O2 positions was checked by refining their occupancy factors; no oxygen vacancies were detected within the standard deviations. In both XRD and NPD patterns, small amounts of an impurity CoO phase were detected, which was included as a second crystallographic phase in the final refinement [CoO is cubic, $a=4.2606(2)$ Å, space group $Fm\text{-}3m$]. From the scale factors a CoO proportion of 4.2(2)% (in weight) was determined. The good agreement between calculated and experimental NPD patterns is shown in Fig. 5. The lattice parameters for $SeCoO_3$ and the reliability factors of the refinement are given in Table I. The atomic positions and some selected atomic distances and bond angles for $SeCoO_3$ are reported in Tables II and III, respectively. A schematic view of the distorted perovskite structure is displayed in Fig. 6. A refinement of the crystallographic structure of $SeCoO_3$ at $T=5$ K has also

TABLE I. Lattice parameters and reliability factors of the NPD refinements carried out at room temperature ($T=295$ K) and $T=5$ K.

| | $T=295$ K | $T=5$ K |
|---|---|---|
| $a$(Å) | 5.9300(2) | 5.9148(2) |
| $a$(Å) | 7.5961(2) | 7.5763(2) |
| $c$(Å) | 5.0287(2) | 5.0217(1) |
| Vol(Å$^3$) | 226.515(11) | 225.033(10) |
| $R_P$(%) | 3.1 | 3.4 |
| $R_{wp}$(%) | 3.8 | 4.4 |
| $R_B$(%) | 13.4 | 8.5 |
| $\chi^2$ | 2.5 | 1.9 |

TABLE II. Interatomic distances (in Å) and some selected bond angles (in deg) for the $CoO_6$ octahedra and $SeO_8$ polyhedra in $SeCoO_3$ at $T=295$ and 5 K.

| | | $T=295$ K | $T=5$ K |
|---|---|---|---|
| | $x$ | 0.0246(4) | 0.0222(4) |
| Se | $z$ | −0.0179(6) | −0.0165(5) |
| | $B$(Å$^2$) | 0.77(5) | 0.55(4) |
| Co | $B$(Å$^2$) | 0.12(11) | 0.17(9) |
| | $x$ | 0.0728(5) | 0.0720(5) |
| O1 | $z$ | 0.3183(7) | 0.3196(6) |
| | $B$(Å$^2$) | 0.56(6) | 0.37(6) |
| | $x$ | 0.1828(4) | 0.1827(3) |
| | $y$ | 0.0774(3) | 0.0772(3) |
| O2 | $z$ | 0.8656(5) | 0.8660(5) |
| | $B$(Å$^2$) | 0.62(4) | 0.43(3) |

been carried out. In the fitting, the magnetic structure of $SeCoO_3$, whose resolution will be presented in the next subsection, has been included. As regarding the CoO impurity phase, the magnetic contribution to the pattern associated to its magnetic order has also been considered, since CoO is an antiferromagnet below $T_N=291$ K.[9,10] The corresponding parameters obtained in the fitting are shown in Tables I–III. The experimental and calculated NPD patterns are compared in Fig. 5.

### *2. Magnetic structure resolution*

The magnetic structure was resolved from a set of NPD patterns acquired in the temperature range 2.2–72.7 K with $\lambda=2.42$ Å. The thermal evolution of the patterns is shown in Fig. 7. On decreasing the temperature below $T_N$, new peaks

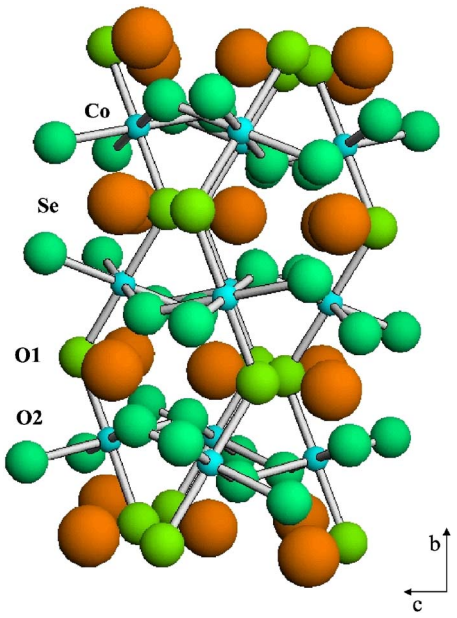


FIG. 6. (Color online) A schematic view of the crystallographic structure of $SeCoO_3$; the $CoO_6$ octahedra are strongly tilted, giving rise to an irregular environment around Se cations (large spheres).

appear in the patterns at Bragg positions forbidden by the space group *Pnma*, in particular, the (100), (001), and (110) reflections are clearly observed. The thermal evolution of the integrated intensity for the magnetic reflections (100) and (110) is presented in Fig. 8. This implies the appearance of a magnetic order below $T_N$, in good agreement with the magnetic measurements. The propagation vector of the magnetic structure is $\mathbf{k}=0$, so the magnetic unit cell coincides with the chemical one. The integrated intensities of the magnetic peaks regularly increase below $T_N$ until achieving saturation,

TABLE III. Interatomic distances (in Å) and some selected bond angles (in deg) for the $CoO_6$ octahedra and $SeO_8$ polyhedra in $SeCoO_3$ at $T=295$ and 5 K.

| | $T=295$ K | $T=5$ K |
|---|---|---|
| Co-O1($x2$) | 2.151(2) | 2.1423(4) |
| Co-O2($x2$) | 2.214(3) | 2.211(2) |
| Co-O2($x2$) | 2.083(2) | 2.078(2) |
| ⟨Co-O⟩ | 2.149(2) | 2.144(2) |
| Se-O1 | 1.715(4) | 1.714(4) |
| Se-O1 | 2.861(4) | 2.840(4) |
| Se-O2($x2$) | 1.715(3) | 1.721(2) |
| Se-O2($x2$) | 2.981(3) | 2.971(3) |
| Se-O2($x2$) | 2.878(3) | 2.861(2) |
| $\langle$Se-O$\rangle_{3short}$ | 1.715(3) | 1.718(3) |
| | Bond angles | |
| Co-O1-Co | 123.96(6) | 124.29(5) |
| Co-O2-Co | 125.02(8) | 125.14(7) |
| Co-O2-Co | 129.55(9) | 129.51(8) |
| O1-Se-O2$_{short}$($x2$) | 104.2(2) | 104.0(2) |
| O1-Se-O2$_{short}$ | 199.7(2) | 99.0(2) |

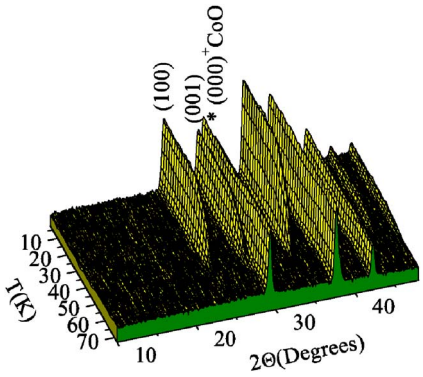


FIG. 7. (Color online) Thermal evolution of the NPD patterns collected with λ=2.42 Å in the temperature interval 2.2–72.7 K. The star indicates the $(000)^+$ magnetic satellite belonging to the CoO impurity.

indicating that the magnetic structure remains stable down to 2.2 K. On the other hand, the analysis of the systematic extinctions demonstrated that only those magnetic peaks with $h+l=2n+1$ are observed.

In the magnetic structure resolution, the possible magnetic modes compatible with the crystallographic structure have been obtained from the group theory representation by following the method described by Bertaut.[11] For the space group *Pnma* and the propagation vector $\mathbf{k}=0$, the different magnetic modes are reported in Ref. 12. The Co atoms are labeled as 1 (0,0,1/2), 2 (1/2,0,0), 3 (0,1/2,1/2), and 4 (1/2,1/2,0). The only basis vectors compatible with the extinction rules are **G** and **A**. After checking the different solutions, the magnetic structure that shows a better agreement with the experimental data is given by the basis vectors

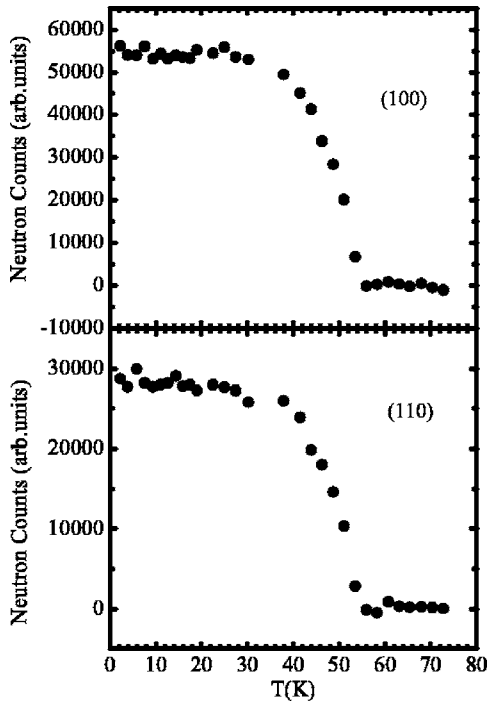


FIG. 8. Thermal variation of the integrated intensities of the magnetic reflections (100) and (110).

TABLE IV. Magnetic structure refinement from NPD patterns collected at $T=2.2$ K with a λ=2.42 Å wavelength.

| | $T=2.2$ K |
|---|---|
| Basis vectors | $(\mathbf{A_x},\mathbf{G_y},0)$ |
| Moment ($\mu_B$) | [2.59(3),−2.15(3),0] |
| $\lvert m\rvert(\mu_B)$ | 3.37(3) |
| $R_B$(Nucl.) | 5.9% |
| $R_B$(Magn.) | 11.2% |
| $\chi^2$ | 2.8 |

$(\mathbf{A_x},\mathbf{G_y},0)$. For this solution, the couplings among the $m_x$ and $m_y$ components of the magnetic moments are $m_{1x}-m_{2x}-m_{3x}+m_{4x}$ (for $\mathbf{A_x}$) and $m_{1y}-m_{2y}+m_{3y}-m_{4y}$ (for $\mathbf{G_y}$). As it is reported in Table IV, at $T=2.2$ K the components of the magnetic moments for Co1 are $m_x=2.59(3)$ $\mu_B$ and $m_y=-2.15(3)$ $\mu_B$, which implies a magnetic moment value $|m|=3.37(3)$ $\mu_B$. In the fitting of the low-temperature NPD patterns the presence of CoO (4.2% in weight) has been considered and both its nuclear and magnetic contribution have been included in the patterns. The magnetic moment for the $Co^{2+}$ cations in CoO refined to 1.0(2) $\mu_B$, and the value remained nearly constant in all the temperature range 2.2–72.7 K. The observed and calculated patterns at $T=2.2$ K are compared in Fig. 9. The thermal evolution of the magnetic moments of the $Co^{2+}$ cations in $SeCoO_3$ is displayed in Fig. 10. As it can be seen in Fig. 11, where the thermal variation of the *a*, *b*, and *c* lattice parameters is shown, *b* remains nearly constant in all the temperature range, where *a* and *c* regularly decrease down to $T_N$, and then remain nearly constant down to 2 K.

A schematic view of the magnetic structure is presented in Fig. 12. As shown, $Co^{2+}$ cations are distributed in (010) layers arranged along the *b* direction. The $Co^{2+}$ magnetic moments are lying on the (*a*,*b*) plane of the perovskite. The magnetic structure is a noncollinear but noncanted arrangement of $Co^{2+}$ moments. In each layer, the magnetic moment of every $Co^{2+}$ cation is antiferromagnetically coupled with respect to the magnetic moments of the four closest neigh-

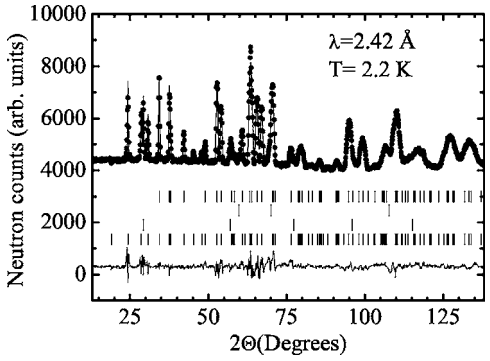


FIG. 9. Experimental (full circles) and calculated (solid line) NPD patterns at $T=2.2$ K. The difference is at the bottom. The first and fourth series of tic marks correspond to the nuclear and magnetic Bragg reflections of $SeCoO_3$, respectively; the second and third ones to the nuclear and magnetic peaks of CoO.

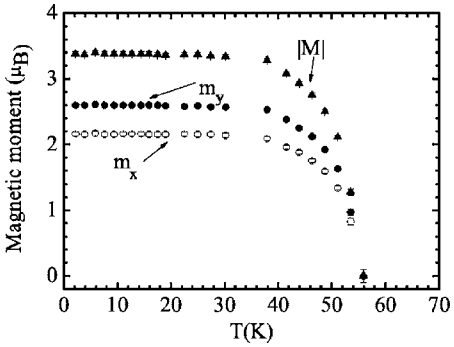


FIG. 10. Thermal evolution of the magnetic moment of $Co^{2+}$ in $SeCoO_3$.

bors. The coupling between the two adjacent (010) layers along $b$ is antiferromagnetic for the $m_x$ component of the magnetic moment, whereas for the $m_y$ component this coupling is ferromagnetic.

## IV. DISCUSSION

The study of the crystallographic structure from high resolution neutron diffraction data confirms that $SeCoO_3$ is a distorted perovskite with an orthorhombic structure, defined in the *Pnma* space group. The values of the unit-cell parameters in the temperature region ranging from RT to 2 K verify the relationship $b/\sqrt{2} > c$ (*Pnma* setting), corresponding to an O-orthorhombic distortion, as it also happens for the members of the series $RCoO_3$ ($R$=rare earth).[13–15] Whereas the $a$ and $b$ lattice parameters of the $SeCoO_3$ result to be larger than those of $RCoO_3$, the $c$ parameter is shorter (*Pnma* setting). The ionic radius of the $Se^{4+}$ cation is 0.64 Å,[16] which is considerably smaller than the corresponding ionic radii for the $R^{3+}$ cations (typically around 1 Å), which gives rise to a huge tilting effect of the $CoO_6$ octahedra in order to optimize the Se-O distances. Co-O-Co angles ($\phi$) are in the range 124°–129.5° (Table II), which are abnormally small in perovskite-related structures. The average tilting angle, estimated as $\varphi=(180-\langle\phi\rangle)/2$ is 26.9°. As a consequence of the strong tilting effect, the oxygen environment of $Se^{4+}$ cations is very irregular, showing three short bond lengths (1.71 Å) and five long bonds in the 2.8–3.0 Å range. These short bonds are expected to be strongly covalent in character; thus, the $SeO_3$ units form discrete entities in $SeCoO_3$, in such a way that, from the chemical point of view, this compound can be named as cobalt selenite. The sterically distorted $SeO_3$ units, forming a trigonal pyramid, are the result of the presence of the nonbonded lone $4s^2$ electron pair, which is thought to be directed towards the apex of each trigonal pyramid. On the other hand, $CoO_6$ octahedra are also distorted, exhibiting short (2.083 Å) and long (2.214 Å) bond lengths on the basal $(a,c)$ plane of the perovskite structure, and medium (2.151 Å) bond lengths in the axial direction of the octahedra, along the $b$ axis (see Fig. 6). This situation may seem reminiscent of the bond length distribution observed in manganese perovskites, $RMnO_3$,[17] where alternating short-long Mn-O distances occurring in the basal plane are explained as a function of the orbital ordering of the two $e_g$ orbitals, only one of them being occupied by an electron. In $SeCoO_3$, with $Co^{2+}$ ions with high spin configuration $t_{2g}^5 e_g^2$, both $e_g$ orbitals contain a single electron, although the same kind of orbital ordering would give rise to slightly stronger $\sigma$ bonds with $d_{3y^2-r^2}$ than $d_{z^2-x^2}$ orbitals, also giving rise to a similar alternating pattern of short and long Co-O bonds.

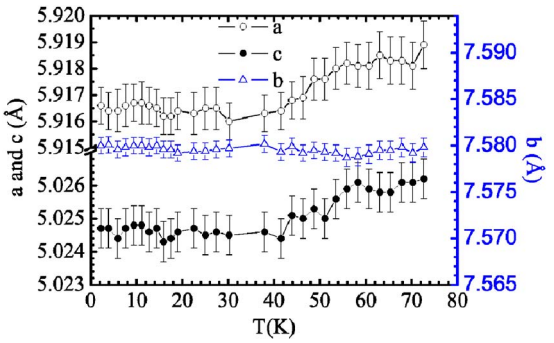


FIG. 11. (Color online) Thermal evolution of the $a$, $b$, and $c$ lattice parameters.

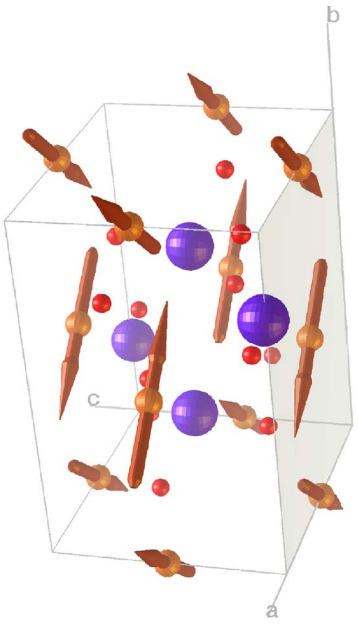


FIG. 12. (Color online) A schematic view of the magnetic structure of $SeCoO_3$. The oxygen and selenium atoms are represented by small and big spheres, respectively.

To account for the results from the magnetic susceptibility data, the electronic configuration $Co^{2+}(3d^7)$ requires a totally unquenched orbital contribution for the high spin $Co^{2+}$ cation, which would explain the large effective moment obtained in the paramagnetic region, well above $T_N$, of $\mu_{\text{eff}}=5.32(1)\ \mu_B$. To establish a comparison, although there are no examples of simple $A^{4+}Co^{2+}O_3$ perovskites, there exists some $Co^{2+}$-containing double perovskites. Recently, Primo-Martin *et al.*[18] studied the $Sr_3CoSb_2O_9$ double perovskite, with an effective moment of 5.39 $\mu_B$ and also proposed a high-spin $Co^{2+}$ configuration with completely unquenched orbital contribution ($^4T_{1g}$ term). This is not an isolated ob-

servation; the double perovskite $Sr_2CoWO_6$ (Ref. 19) also exhibited a paramagnetic moment of 5.20 $\mu_B$, and the oxides $A_2CoTeO_6$ (Ref. 20) showed effective moments of 5.50 $\mu_B$/f.u. and 5.48(2) $\mu_B$/f.u. for $A$=Ca, Sr, respectively. Moreover, many simple $Co^{2+}$ compounds display effective moments between 3.87 $\mu_B$ (spin only) and 5.20 $\mu_B$ (spin plus completely unquenched orbital contribution);[21,22] some examples are $CoF_2$ ($\mu_{eff}$=5.15 $\mu_B$) or CoO ($\mu_{eff}$=5.1 $\mu_B$).

The magnetization and specific heat measurements have shown that $SeCoO_3$ exhibits an antiferromagnetic ordering below $T_N \approx 54$ K. On the other hand, the neutron diffraction experiments reveal that the magnetic structure below $T_N$ is given by the basis vector $(\mathbf{A_x}, \mathbf{G_y}, 0)$. The magnetic unit cell coincides with the chemical one ($\mathbf{k}$=0), and the magnetic structure remains stable down to 2.2 K. At $T$=2.2 K, the ordered magnetic moment value for the $Co^{2+}$ ions is $|m|$ =3.37(3) $\mu_B$, which is slightly higher than that expected for spin-only $Co^{2+}$ cations, in the high spin electronic configuration $t_{2g}^5 e_g^2$ (3 $\mu_B$ per $Co^{2+}$ ion). The obtained magnitude suggests that the orbital magnetic moment is only partially quenched, as it usually happens in the Co cations. The magnetic structure (Fig. 12) corresponds to a noncollinear, antiferromagnetic arrangement of $Co^{2+}$ magnetic moments. Within the $(a,c)$ planes the coupling of each $Co^{2+}$ cation with its four closer neighbours is purely antiferromagnetic (180°). Between adjacent layers the magnetic coupling is more complex: for the $x$ component of the magnetic moment along $a$ it is also antiferromagnetic, whereas for the $y$ component the coupling is ferromagnetic, as displayed in Fig. 12. The superexchange Co-O2-Co interaction within (010) layers can be understood according to the Goodenough-Kanamori rules[23–25] taking place through alternating, half-occupied $d_{z^2-x^2}$ and $d_{3y^2-r^2}$ orbitals, via intermediate oxygen $2p$ orbitals, implying a negative exchange parameter and a purely antiferromagnetic interaction. Between (010) layers the observed magnetic coupling implies an admixture of antiferromagnetic and ferromagnetic interactions, along Co-O1-Co paths. The direct superexchange interaction via half-occupied Co $d_{z^2-x^2}$ orbitals would be antiferromagnetic for an ideal Co-O-Co angle of 180°. It is well known that in structures containing intermediate cation-anion-cation angles (between 180° and 90°) the sign of the interaction changes from antiferromagnetic to ferromagnetic as the angles become closer to 90°. A related example is that of the series $Se_{1-x}Te_xCuO_3$,[2] where the magnetic interactions may be tuned from AFM ($x$=1) to FM ($x$=0) by decreasing the tolerance factor of the perovskite structure as the Te content decreases. The FM interactions are usually triggered below a critical angle, which can change from system to system. In our case, $SeCoO_3$ crystal structures show abnormally small Co-O1-Co angles along the $b$ direction of 123.9°; for this narrow superexchange angle the FM interactions are plausible to appear and partially straighten the moments direction along Co-O1-Co infinite chains, giving rise to the observed AFM+FM admixture from layer to layer. The microscopic reason for the appearance of such FM interactions for very bent bond angles can be found in the direct overlapping between $t_{2g}$ orbitals of neighboring $Co^{2+}$ cations giving rise to the "delocalization superexchange" defined by Goodenough.[24] In this mechanism an electron is assumed to drift from one cation to the other, the transfer integral depending on the amount of direct overlap of $t_{2g}$ cation orbitals, which is enhanced for extremely bent Co-O-Co angles. The delocalization superexchange is ferromagnetic between half-filled and filled $t_{2g}$ orbitals, which are present for the high-spin $Co^{2+}$ configuration, $t_{2g}^5 e_g^2$.

## V. CONCLUSION

$SeCoO_3$ crystallizes in an O-orthorhombic distorted perovskite structure, where the strongly tilted $CoO_6$ octahedra show an average rotation angle of 26.9°. The Co-O bond distances in the $CoO_6$ polyhedron are rather different, with the longest and shortest bond distances to O2 oxygens lying in the equatorial plane and the medium bond length to O1 along the apical direction. $Se^{4+}$ is coordinated to three oxygens in a very irregular environment, forming $SeO_3$ trigonal pyramidal units, due to the presence of the $Se^{4+}$ electron lone pair. The susceptibility measurements show the onset of an antiferromagnetic order below $T_N$ 54 K. The magnetic structure, studied from NPD data, is characterized by the propagation vector $\mathbf{k}$=0. The spin arrangement is given by the basis vectors $(\mathbf{A_x}, \mathbf{G_y}, 0)$, defining a noncollinear but noncanted structure. In the $(a,c)$ planes the coupling of the magnetic moments for each Co atom with its four closer neighbors is purely antiferromagnetic. For the $x$ component of the magnetic moment the coupling between the (010) layers along $b$ is antiferromagnetic, whereas for the $y$ component the coupling is ferromagnetic, which can be understood according to the Goodenough-Kanamori rules. At $T$=2.2 K, the ordered magnetic moment for $Co^{2+}$ ions is $|m|$=3.37(3) $\mu_B$, suggesting a high-spin electronic configuration for $Co^{2+}$ cations, $t_{2g}^5 e_g^2$, with some component of unquenched orbital moment.

## ACKNOWLEDGMENTS

We thank the financial support of Spanish CICyT to the projects Nos. MAT2004-0479, MAT2005-06024-C02-01, and MAT2004-1641, and we are grateful to ILL for making all facilities available.

*Electronic address: amunoz@fis.uc3m.es

[1] K. Kohn, K. Imoue, O. Horie, and S. Akimoto, J. Solid State Chem. **18**, 9 (1976).

[2] M. A. Subramanian, A. P. Ramirez, and W. J. Marshall, Phys. Rev. Lett. **82**, 1558 (1999).

[3] G. Lawes, A. P. Ramirez, C. M. Varma, and M. A. Subramanian, Phys. Rev. Lett. **91**, 257208 (2003).

[4] R. Escamilla, A. Duràn, M. I. Rosales, E. Moràn, and M. A.

Alario-Franco, J. Phys.: Condens. Matter **15**, 1951 (2003).
[5] A. Villesuzanne, M. H. Whangbo, M. A. Subramanian, and S. F. Matar, Chem. Mater. **17**, 4350 (2005).
[6] H. M. Rietveld, J. Appl. Crystallogr. **2**, 65 (1969).
[7] J. Rodríguez-Carvajal, Physica B **192**, 55 (1993).
[8] W. L. Roth, J. Phys. Chem. Solids **1**, 25 (1964).
[9] S. Greenwald, Acta Crystallogr. **6**, 396 (1953).
[10] W. C. Roth, Phys. Rev. **110**, 1333 (1958).
[11] E. F. Bertaut, Acta Crystallogr., Sect. A: Cryst. Phys., Diffr., Theor. Gen. Crystallogr. **24**, 217 (1968).
[12] A. Muñoz, J. A. Alonso, M. J. Martínez-Lope, J. L. García-Muñoz, and M. T. Fernández-Díaz, J. Phys.: Condens. Matter **12**, 1361 (2000).
[13] J. S. Zhou and J. B. Goodenough, Phys. Rev. Lett. **94**, 065501 (2005).
[14] C. Y. Chang, B. N. Lin, H. C. Ku, and Y. Y. Hsu, Chin. J. Phys. (Taipei) **41**, 662 (2003).
[15] X. Liu and C. T. Prewitt, J. Phys. Chem. Solids **52**, 441 (1991).
[16] R. D. Shannon, Acta Crystallogr., Sect. A: Cryst. Phys., Diffr., Theor. Gen. Crystallogr. **32**, 751 (1976).
[17] J. A. Alonso, Martínez-Lope, M. T. Casais, and M. T. Fernández-Díaz, Inorg. Chem. **39**, 917 (2000).
[18] V. Primo-Martin and M. Jansen, J. Solid State Chem. **157**, 76 (2001).
[19] M. C. Viola, M. J. Martínez-Lope, J. A. Alonso, J. L. Martínez, J. M. De Paoli, S. Pagola, J. C. Pedregosa, M. T. Fernández-Díaz, and R. E. Carbonio, Chem. Mater. **15**, 1655 (2003).
[20] M. S. Augsburger, M. C. Viola, J. C. Pedregosa, A. Munoz, J. A. Alonso, and R. E. Carbonio, J. Mater. Chem. **15**, 993 (2005).
[21] R. J. Radwanski and Z. Ropka, Physica B **281-282**, 507 (2000).
[22] A. Mahendra and D. C. Khan, Phys. Rev. B **4**, 3901 (1971).
[23] J. B. Goodenough, Phys. Rev. **100**, 564 (1955).
[24] J. B. Goodenough, *Magnetism and the Chemical Bond* (Wiley, New York, 1963).
[25] J. Kanamori, J. Phys. Chem. Solids **10**, 87 (1959).